RESEARCH ARTICLE

Yuqi LIU*, Yitong LIU*, Yue YU, Chengzhan LIU, Shuangxi XING

Facile route to achieve MoSe₂-Ni₃Se₂ on nickel foam as efficient dual functional electrocatalysts for overall water splitting

Abstract   Since the catalytic activity of present nickel-based synthetic selenide is still to be improved, $MoSe_2$-Ni_3Se_2 was synthesized on nickel foam (NF) ($MoSe_2$-Ni_3Se_2/NF) by introducing a molybdenum source. After the molybdenum source was introduced, the surface of the catalyst changed from a single-phase structure to a multi-phase structure. The catalyst surface with enriched active sites and the synergistic effect of $MoSe_2$ and Ni_3Se_2 together enhance the hydrogen evolution reactions (HER), the oxygen evolution reactions (OER), and electrocatalytic total water splitting activity of the catalyst. The over-potential of the $MoSe_2$-Ni_3Se_2/NF electrocatalyst is only 259 mV and 395 mV at a current density of 100 mA/cm² for HER and OER, respectively. $MoSe_2$-Ni_3Se_2/NF with a two-electrode system attains a current density of 10 mA/cm² at 1.60 V. In addition, the overpotential of HER and OER of $MoSe_2$-Ni_3Se_2/NF within 80000 s and the decomposition voltage of electrocatalytic total water decomposition hardly changed, showing an extremely strong stability. The improvement of $MoSe_2$-Ni_3Se_2/NF catalytic activity is attributed to the establishment of the multi-phase structure and the optimized inoculation of the multi-component and multi-interface.

Keywords   three-dimensional molybdenum nanomaterials, hydrogen evolution reaction, oxygen evolution reaction, overall water splitting

Yuqi LIU , Yitong LIU , Chengzhan LIU, Shuangxi XING (✉)
Faculty of Chemistry, Northeast Normal University, Changchun 130024, China
E-mail: xingsx737@nenu.edu.cn

Yue YU
College of Chemistry and Chemical Engineering, Neijiang Normal University, Neijiang 641100, China

*The two authors contribute equally in this work.

1   Introduction

The rapid economic development based on fossil fuels greatly intensifies environmental pollution and energy crises, prompting the exploration of sustainable clean energy [1–4]. As an energy source, hydrogen has the advantages of high energy density, environmental friendliness, and renewability, thus has the potential to replace fossil fuels [5–7]. An effective strategy for hydrogen production is overall water splitting and it is one of the energy conversion methods with a great application potential. Renewable energy such as solar energy can drive overall water splitting [8–13]. Hydrogen production by overall water splitting is resulted from the hydrogen and oxygen evolution reactions (HER, OER), reacting at the cathode and the anode, respectively. The number which shows 1.23 V in decomposition voltage water is theoretical. However, due to the sluggish kinetics and the impact of electrolyte chemistry, the actual decomposition voltage is much larger than 1.23 V [14–16]. Currently, commercialized hydrogen evolution catalysts, such as Pt, and oxygen evolution catalysts, such as RuO_2 with superior performances are low-reserve in nature and expensive, which greatly limits their applications [17,18]. Therefore, research on the low-cost catalyst with a better activity and stability in the improvement of overall water splitting technology is indispensable.

Up to the present, many types of low-cost electrocatalysts with superior performances and good catalytic stabilities have been developed, including molybdenum [19–21], iron [22–24], cobalt [25–28], nickel [29–34], and vanadium-based [35,36] compounds, of which, more attention have been paid to nickel-based compounds in storage and conversion of energy owing to their high abundance in nature, easy access, and low price. The density functional theory results illustrate that Se doping is beneficial for decreasing the kinetic barrier and the free energy of HER. Nickel-based selenide with specific phases

has been reported to have a good electrocatalytic activity, but it still needs great improvement in order to meet the practical requirement [37,38]. A variety of strategies have been adopted to develop the electrochemical water splitting activity of nickel-based selenide, including heteroatom doping [39], phase change [40], and combination with conductive substrates [41,42], such as carbon nanotubes, conductive graphene, etc.

In this work, by using nickel foam (NF) as the substrate, $MoSe_2$-Ni_3Se_2/NF multiphase composite material was prepared by utilizing a one-pot hydrothermal method. As a result, the activity of the modified electrocatalyst was increased significantly for HER and OER. The $MoSe_2$-Ni_3Se_2/NF electrocatalyst showed an unexceptionable activity with an overpotential of only 259 mV and 395 mV for HER and OER at a current density of 100 mA/cm^2, respectively. In addition, when assembled in a two-electrode system, the $MoSe_2$-Ni_3Se_2/NF electrocatalyst could reach a current density of 10 mA/cm^2 with an overpotential of 1.60 V for overall water splitting.

2 Experimental

2.1 Materials

The selenium powder was purchase from Aladdin. The ammonium heptamolybdate tetrahydrate (AHT), commercial Pt/C (20% (mass ratio)), and RuO_2 were purchased from Tianjin Kaida Chemical Plant, Shanghai Hesen Electric Co., Ltd., and Sigma-Aldrich, respectively. The acetone, hydrazine hydrate solution, and ethanol were purchased from Beijing Chemical Plant. The foam nickel (NF) was purchased from Guangdong Candlelight New Energy Technology Co., Ltd. All experiments were conducted using deionized water (deionized water, 18.25 MΩ·cm).

2.2 Synthesis of $MoSe_2$-Ni_3Se_2/NF, Ni_3Se_2/NF, Pt/C-NF, and RuO_2-NF

To remove the oxide layer, the NF substrate was soaked in an acetone solution for 24 h. Then, it was taken out, ultrasonically cleaned in ethanol and DI water for 30 min, and dried it in an oven at 50°C overnight. The selenium powder (0.1575 g) was dispersed in 10 mL of hydrazine hydrate solution and stirred for 5 h until the solution turns brown-black. Meanwhile, the AHT (0.1765 g) was dispersed in 50 mL of DI water and stirred for 30 min until the particles were completely dissolved. Under stirring, the selenium solution was slowly added into the AHT solution drop by drop, and then stirred for 30 min. The reaction mixture was shifted to a 100 mL autoclave reactor with a piece of NF (2 cm× 5 cm). Then, the autoclave was put into an oven and sintered at 200°C for 20 h. After that, the reactor was moved out and cooled

down naturally. The resultant NF-supported catalyst was ultrasonically washed with DI water and ethanol, and dried at 50°C overnight. The product which was obtained by the experience was recorded as $MoSe_2$-Ni_3Se_2/NF. For comparison, the Ni_3Se_2/NF was prepared following the same steps, but without introducing AHT. The Pt/C or RuO_2 loaded samples were prepared by weighing 4 mg of Pt/C and RuO_2 in two sorts of sample tubes, containing 190 μL of isopropanol, 50 μL of naphthol, 380 μL of deionized water, and 380 μL of ethanol. The mixture was kept ultrasonicating for 30 min. Finally, 200 μL of the above ink was evenly smeared on the top layer of NF (1 cm × 1 cm). The catalyst loading rate on the sample is approximately 0.8 mg/cm^2.

2.3 Physical characterization

X-ray diffraction (XRD) analysis was performed on Siemens D5005 diffractometer with Cu-Kα source ($\lambda = 1.5418$ Å) at 40 kV and 30 mA, and a scan rate of 5 (°)/min. Scanning electron microscope (SEM) and (high resolution-) transmission electron microscopy (TEM (100 kV), HR-TEM (200 kV)) pictures were obtained by using the JEOL SM-6360LV field emission scanning electron microscope and the JEOL JSM-2100F driving device electron microscope, respectively. In addition, a field emission transmission electron microscope (Tecnai G2 F-30 S-TWIN) was used to conduct the elemental analysis. X-ray photoelectron spectroscopy (XPS) was performed through the ESCALAB 250 spectrometer by a mono-chromatic Al Kα X-ray source (1486.6 eV).

2.4 Electrochemical characterization

All electrochemical experiments were conducted via the CHI660E electrochemical workstation, using the 1.0 mol/L aqueous KOH electrolyte solution. A three-electrode cell with the catalyst-supported NF (0.5 cm × 0.5 cm) was used as the working electrode, while the Hg/HgO electrode and carbon rod were used as the reference and counter electrodes, respectively. Before experiencing the electrocatalytic performance, the electrolyte was filled with nitrogen or oxygen for 30 min. The reference potential of HER and OER was modified by $E_{RHE} = E_{Hg/HgO} + 0.059$ pH $+ 0.099$ V. The polarization curve (LSV) was recorded at a scan rate of 5 mV/s, and each electrode was iR (85%) corrected to eliminate the effect of the internal obstruction of the solution. The cyclic voltammetry (CV) was performed at a sweep speed of 20, 40, 60, 80, and 100 mV/s. The electrochemical impedance spectroscopy (EIS) was evaluated in the frequency range of 100 kHz to 0.1 Hz. The stability tests were performed by chronopotentiometry at an invariable current of 10 mA/cm^2 for HER, OER, and total water splitting (80000 s). The electrocatalytic water splitting experiment was conducted in a two-electrode battery, with
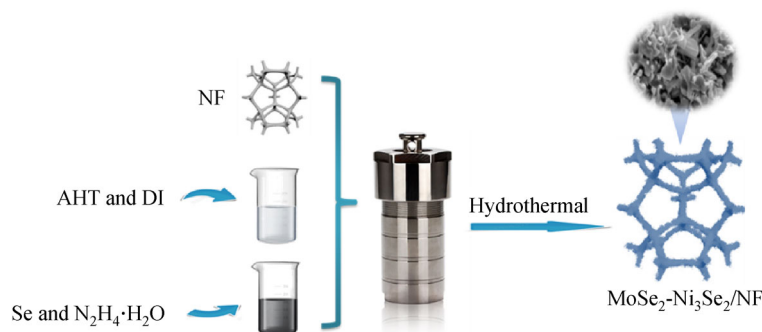
Fig. 1   Synthesis process of MoSe$_2$-Ni$_3$Se$_2$/NF.

MoSe$_2$-Ni$_3$Se$_2$/NF (0.5 cm × 0.5 cm) as the cathode and anode.

The Faraday efficiency (*FE*) is calculated by

$$FE(\%) = n_{\mathrm{Exp}}/n_{\mathrm{Theo}}, \tag{1}$$

where n_{Exp} means the total number of moles of the collected H$_2$ and O$_2$ gases and $n_{\mathrm{Theo}} = 3Q/(4F)$ (Q is the charge passing through the electrodes and F is Faraday constant).
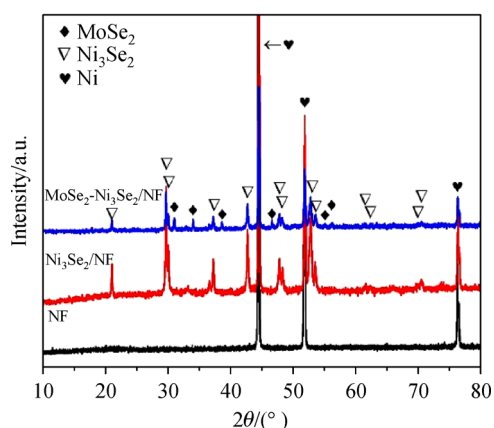
3   Results and discussion

MoSe$_2$-Ni$_3$Se$_2$/NF synthesized by the method is shown in Fig. 1, while the XRD patterns of Ni$_3$Se$_2$/NF and MoSe$_2$-Ni$_3$Se$_2$/NF are demonstrated in Fig. 2. The characteristic peaks of the nickel matrix correspond to three strong diffraction peaks at 44.58°, 51.96°, and 76.43° [43]. The main diffraction peaks at 21.09°, 29.65°, 36.78°, 37.25°, 42.76°, 47.80°, 48.38°, 52.75°, 53.60°, 61.67°, 62.63°, 69.96°, 70.61° correspond to the characteristic peaks of Ni$_3$Se$_2$ (JCPDS No.19-0841) [42]. Upon addition of AHT, the crystalline phase of MoSe$_2$ appears with the main diffraction peaks at 30.98°, 34.01°, 38.67°, 46.65°, 55.11°,
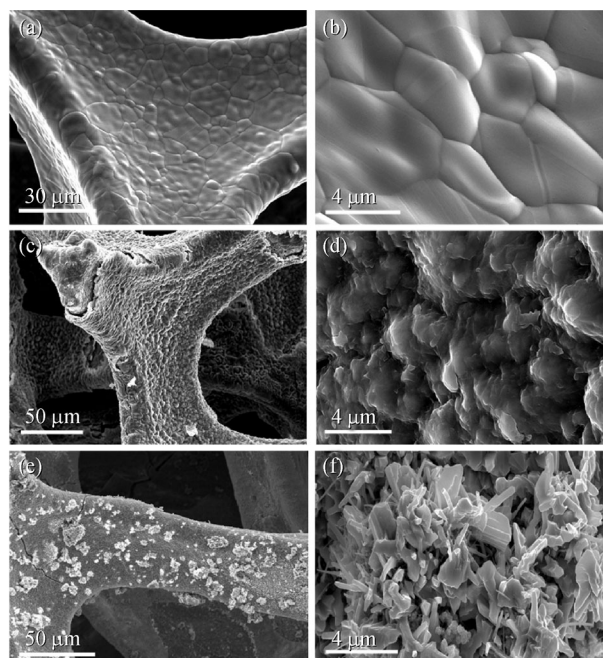
and 56.26°, corresponding to the characteristic peaks of MoSe$_2$ (JCPDS No.29-0914) [44].

Figures 3(a) and 3(b) illustrate the smooth surface of NF after pretreatment. Upon addition of the selenium powder, the obtained Ni$_3$Se$_2$/NF gives a uniform single-phase structure (Figs. 3(c) and 3(d)). However, if the selenium powder and ammonium molybdate tetrahydrate are simultaneously introduced, the NF surface generate a multiphase structure (Figs. 3(e) and 3(f)). The formation of the MoSe$_2$-Ni$_3$Se$_2$/NF composite structure leads to an increase in the specific surface area of the electrocatalyst, which supplies more active sites and accelerates the electron transport.
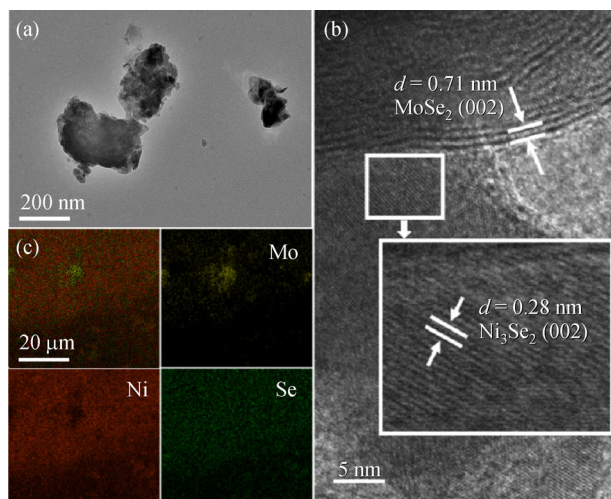
The morphology of the MoSe$_2$-Ni$_3$Se$_2$/NF is further investigated via TEM which suggests that the composite has a non-uniform nanosheet structure (Fig. 4(a)). In the corresponding HRTEM image, the (002) crystal plane of

Fig. 3   SEM images at different resolutions.
(a, b) NF; (c, d) Ni$_3$Se$_2$/NF; (e, f) MoSe$_2$-Ni$_3$Se$_2$/NF.

Fig. 2   XRD patterns of NF, Ni$_3$Se$_2$/NF, MoSe$_2$-Ni$_3$Se$_2$/NF.

Fig. 4 TEM images at different resolutions.
(a) TEM images of MoSe$_2$-Ni$_3$Se$_2$/NF; (b) HRTEM images of MoSe$_2$-Ni$_3$Se$_2$/NF; (c) corresponding elemental mapping of MoSe$_2$-Ni$_3$Se$_2$/NF.

Ni$_3$Se$_2$ can get lattice fringes with a pitch of about 0.28 nm [45], and the (012) crystal plane of MoSe$_2$ can get lattice fringes with a pitch of about 0.71 nm [44]. In addition, the element map in Fig. 4(c) manifests that Ni, Se, and Mo are uniformly distributed on the surface of MoSe$_2$-Ni$_3$Se$_2$/NF.

The energy dispersive spectroscopy spectra of the sample and the corresponding images are given in Electronic Supplementary Material (Fig. S1). The content of Mo, Ni, and Se are 6.48%, 75.29%, 18.23% respectively, which reveals the even distribution of Ni, Se and Mo on the surface of MoSe$_2$-Ni$_3$Se$_2$/NF.

The surface chemical state and electronic properties of MoSe$_2$-Ni$_3$Se$_2$/NF electrocatalysts were evaluated by XPS. Figure 5(a) exhibits that the main elements of the MoSe$_2$-Ni$_3$Se$_2$/NF electrocatalyst are Ni, Mo, and Se (Fig. 5(a)) [46]. In Fig. 5(b), after deconvolution of Ni 2p, the six peaks at 852.34, 855.60, 861.25, 869.30, 873.30, and 879.34 eV correspond to Ni^0, Ni^{2+} 2p$_{3/2}$, satellite peak, Ni^0, Ni^{2+} 2p$_{1/2}$, and satellite peak, respectively [21]. The peaks at 228.60 eV and 231.67 eV correspond to 3d$_{5/2}$ and 3d$_{3/2}$ of Mo^{4+}, respectively. The peaks at 232.09 eV and 235.07 eV correspond to Mo^{6+}. The presence of the peak of Mo^{6+} on the surface of the electrocatalyst may be due to the slight oxidation of air (Fig. 5(c)) [46]. The peaks at 54.05 eV and 55.15 eV correspond to Se 3d$_{5/2}$ and 3d$_{3/2}$, respectively. In addition, a strong peak at 58.72 eV corresponding to SeO$_x$ is observed, which may be caused by the air exposure [21] (Fig. 5(d)).

Figure 6(a) displays the electrocatalytic activity of the samples in the 1.0 mol/L KOH solution. When voltage is applied to the cathode, the LSV curve of MoSe$_2$-Ni$_3$Se$_2$/NF indicates that the current density is increasing sharply.
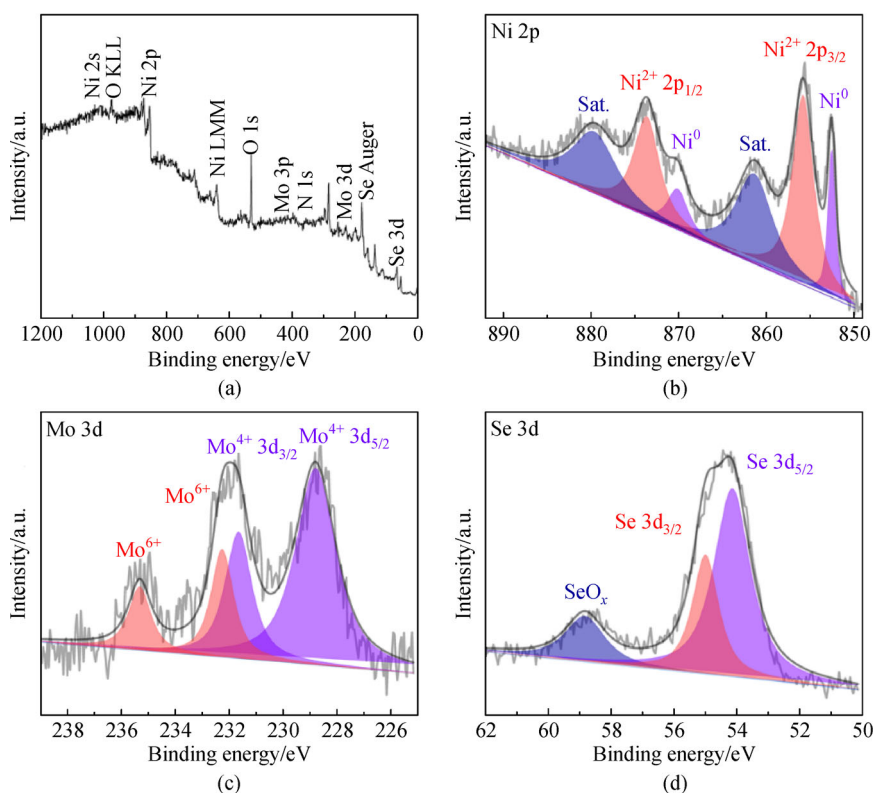
Fig. 5 XPS total spectrum.
(a) MoSe$_2$-Ni$_3$Se$_2$/NF; (b) Ni 2p; (c) Mo 3d; (d) Se 3d high-resolution XPS spectra.
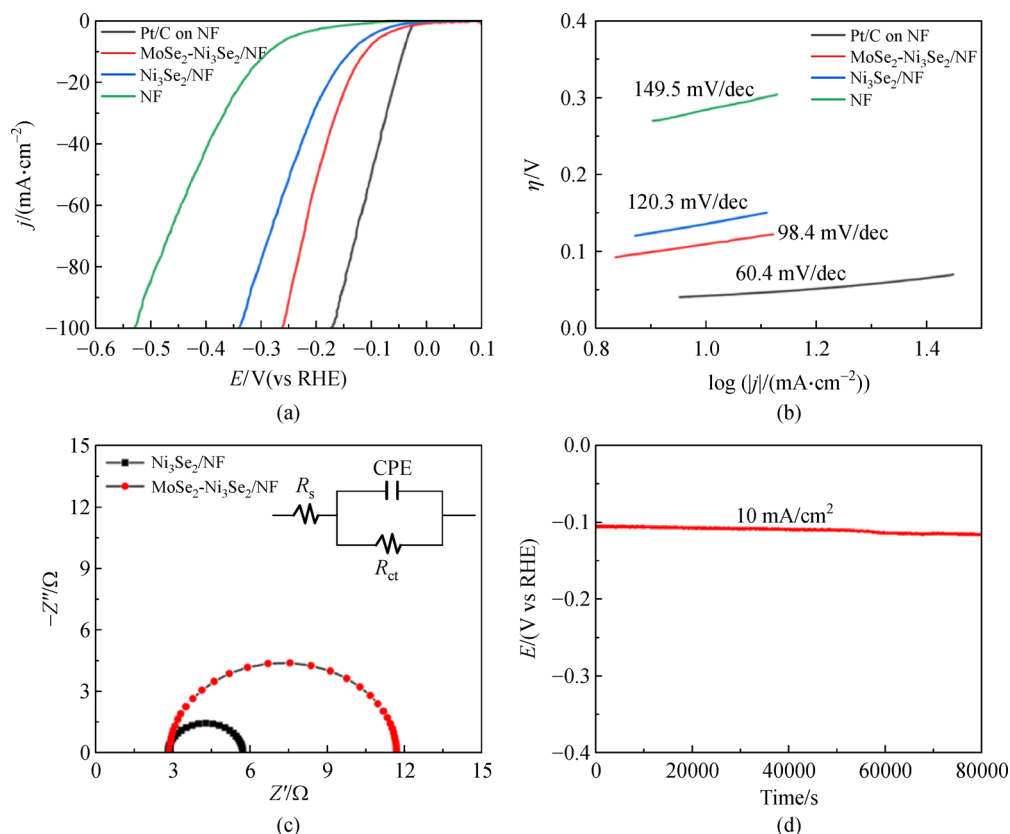
Fig. 6 Electrochemical characterization of HER.
(a) LSV curves; (b) Tafel plots of MoSe$_2$-Ni$_3$Se$_2$/NF, Ni$_3$Se$_2$/NF, NF and Pt/C for HER; (c) Nyquist plots (at η = 100 mV, the equivalent circuit of the EIS fitting result is based on inline image); (d) chronoamperometry response at η = 10 mA/cm^2 (MoSe$_2$-Ni$_3$Se$_2$/NF) for HER in a 1.0 mol/L KOH.

The overpotential at 10 and 100 mA/cm^2 is only 106 and 259 mV, respectively. For comparison, the LSV curve of the Pt/C-NF exhibits a lowest overpotential (η_{10} = 45 mV and η_{100} = 169 mV). On the contrary, the commercial NF and Ni$_3$Se$_2$/NF demonstrate an overpotential of 285 and 136 mV at 10 mA/cm^2, respectively, which confirms the advantage of introducing AHT. Another important basis to evaluate the catalytic performance of an electrocatalyst is the Tafel slope. As the HER catalytic activity of a sample improves, the Tafel slope decreases [47–49]. At present, the HER electron reflection model has been generally mentioned as

Volmer reaction:

$$H_2O \ (aq) + e^- + * \rightarrow H* + OH^-(aq), \qquad (2)$$
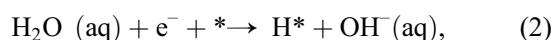
Heyrovsky reaction:

$$H* + H_2O \ (aq) + e^- \rightarrow H_2 + OH^-(aq) + *, \qquad (3)$$
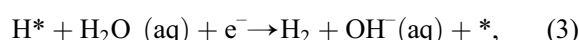
Tafel reaction: $H* + H* \rightarrow H_2 + 2*$. $\qquad (4)$

The Tafel slopes of commercial NF, Ni$_3$Se$_2$/NF, MoSe$_2$-Ni$_3$Se$_2$/NF and commercial Pt/C on NF are 149.5, 120.3,
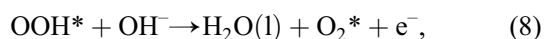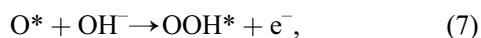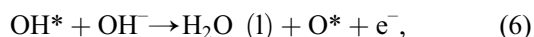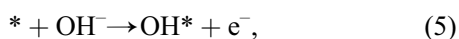
98.4, and 60.4 mV/dec (Fig. 6(b)), revealing the excellent HER performance of MoSe$_2$-Ni$_3$Se$_2$/NF. The electrocatalytic active surface area of the electrocatalyst was evaluated by measuring the electric double layer capacitance of the sample. As the electric double layer capacitance value increases, the number of active groups on the catalyst surface increases, too [50,51]. The C_{dl} value of MoSe$_2$-Ni$_3$Se$_2$/NF is 38.8 mF/cm^2 (Fig. S2(a), S2(b)), while the C_{dl} value of Ni$_3$Se$_2$/NF is only 7.9 mF/cm^2 (Figs. S2(c), S2(d)) [52]. The EIS of the sample was further measured to analyze the HER kinetic process of the electrocatalyst. The R_{ct} value is inversely proportional to the HER kinetic rate and electron transfer rate [53,54]. As shown in Fig. 6(c), the R_{ct} value of MoSe$_2$-Ni$_3$Se$_2$/NF is much smaller than that of Ni$_3$Se$_2$/NF, which may be attributed to the improved electron transfer efficiency of MoSe$_2$-Ni$_3$Se$_2$/NF with a multiphase surface structure, in contrast to the single-phase structure of Ni$_3$Se$_2$/NF.

In the long term stability test, the overpotential of the MoSe$_2$-Ni$_3$Se$_2$/NF composite material hardly changes within 80000 s (Fig. 6(d)), which, therefore, demonstrates the satisfactory durability of the MoSe$_2$-Ni$_3$Se$_2$/NF composite.

The OER activity of MoSe$_2$-Ni$_3$Se$_2$/NF, Ni$_3$Se$_2$/NF and

commercial RuO_2-NF and NF was evaluated in the 1.0 mol/L KOH solution. The overpotential of $MoSe_2$-Ni_3Se_2/NF at 100 mA/cm^2 is 395 mV, comparable to the activity of commercial RuO_2-NF with an overpotential of 341 mV. However, the overpotential of Ni_3Se_2/NF and NF at 100 mA/cm^2 is 455 and 500 mV, respectively (Fig. 7(a)). The OER activity of the catalyst was also evaluated by Tafel plot. The OER reaction process is more complicated. The currently recognized reaction process is shown as

$$* + OH^- \rightarrow OH* + e^-, \tag{5}$$

$$OH* + OH^- \rightarrow H_2O \ (l) + O* + e^-, \tag{6}$$

$$O* + OH^- \rightarrow OOH* + e^-, \tag{7}$$

$$OOH* + OH^- \rightarrow H_2O(l) + O_2* + e^-, \tag{8}$$

$$O_2* \rightarrow * + O_2. \tag{9}$$

The Tafel slopes of $MoSe_2$-Ni_3Se_2/NF, Ni_3Se_2/NF, and RuO_2-NF and NF are 62.3, 87.6, 42.4, and 102.6 mV/dec, respectively (Fig. 7(b)). In Fig. 7(c), the EIS test reveals that $MoSe_2$-Ni_3Se_2/NF has a lower R_{ct} value than Ni_3Se_2/NF.

In addition, the stability of $MoSe_2$-Ni_3Se_2/NF is also implemented by chronoamperometry, which almost does not change in the overpotential of $MoSe_2$-Ni_3Se_2/NF at 10 mA/cm^2 within 80000 s (Fig. 7(d)). Thus, the $MoSe_2$-Ni_3Se_2/NF has a satisfactory catalytic durability under alkaline conditions.

There are two reasons for improving the performance of HER and OER. The first reason is that introduction of the molybdenum source leads to the surface reconstruction of the catalyst (transformation from a single-phase structure to a multi-phase structure), which supply more active sites and speeds up the electron transfer efficiency. The second reason is that with the introduction of molybdenum source, a multi-component multi-interface electrocatalyst is formed, which may lead to an increase in the electro-catalytic activity.

Based on the excellent HER and OER activities of $MoSe_2$-Ni_3Se_2/NF, two electrode cells are assembled for total water splitting. The result shows that the required full water decomposition voltage is only 1.60 V at 10 mA/cm^2 (Fig. 8(a)). In contrast, the electrocatalytic water splitting voltage of Pt/C-NF|RuO_2-NF and Ni_3Se_2/NF is 1.53 and 1.66 V at a current density of 10 mA/cm^2, respectively.
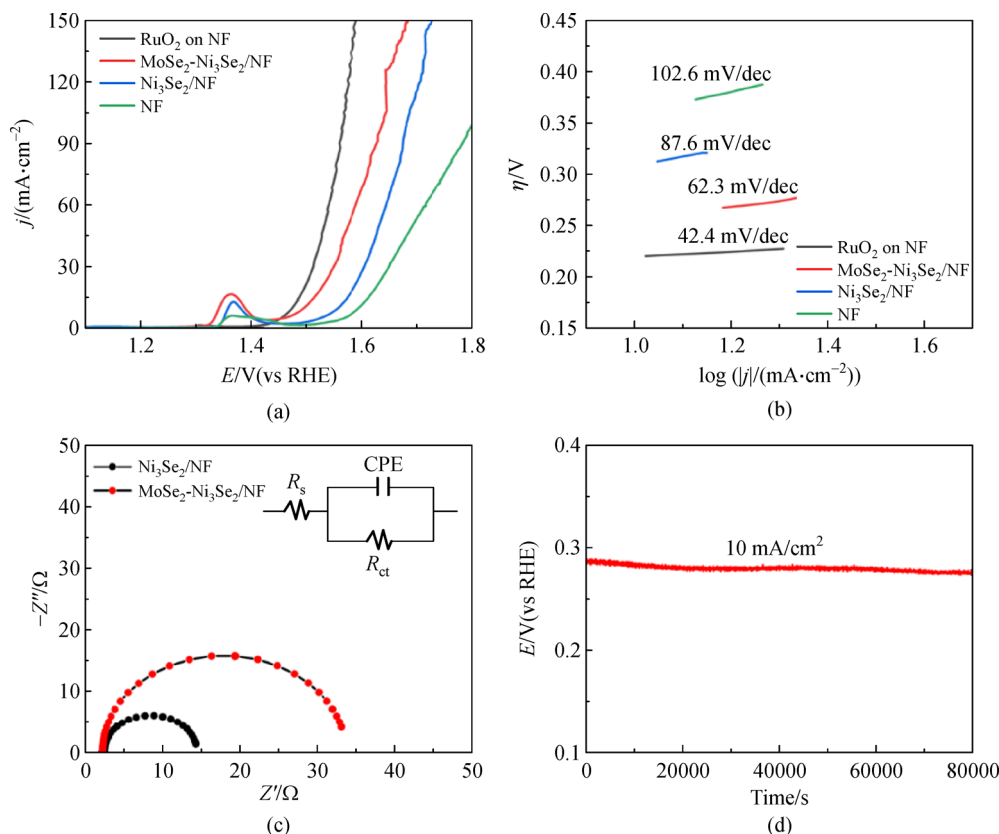
Fig. 7 Electrochemical characterization of OER.

(a) LSV response curves; (b) Tafel plots of $MoSe_2$-Ni_3Se_2/NF, Ni_3Se_2/NF, NF and Pt/C for OER; (c) Nyquist plots (at $\eta = -0.2$ V versus RHE, the equivalent circuit of the EIS fitting result is based on inline image); (d) long-term durability tests at $\eta = 10$ mA/cm^2 ($MoSe_2$-Ni_3Se_2/NF) for OER in a 1.0 mol/L KOH electrolyte.
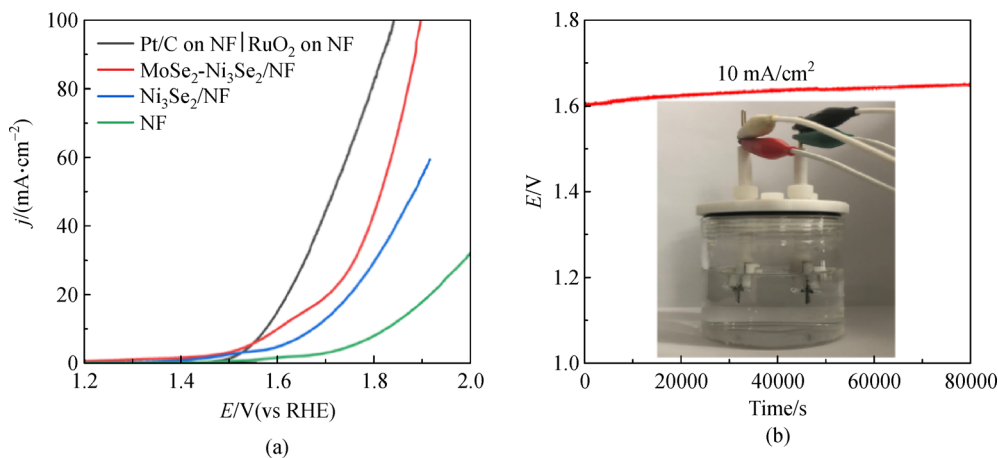
Fig. 8 Electrochemical characterization of overall water splitting.
(a) Polarization curves; (b) long-term durability tests at 1.60 V of MoSe$_2$-Ni$_3$Se$_2$/NF for total water splitting in a 1.0 mol/L KOH solution.

In addition, the durability of MoSe$_2$-Ni$_3$Se$_2$/NF for electrocatalytic water splitting was also evaluated by chronoamperometry at 10 mA/cm^2. After 80000 s, the overall water splitting voltage of MoSe$_2$-Ni$_3$Se$_2$/NF hardly changed, indicating its good potential in practical application (Fig. 8(b)). Meanwhile, under the condition of 10 mA/cm^2, the total water decomposition activity of MoSe$_2$-Ni$_3$Se$_2$/NF in lake water (our school lake water) was tested. At 10 mA/cm^2, the overpotential of the sample is 1.62 V (Fig. (9)), close to the overpotential in deionized water, indicating that it has a great practical application value. Through testing and calculation, the Faraday efficiency of HER and OER of the electrocatalyst is provided in Electronic Supplementary Material; the calculation results show that the Faraday efficiency of the catalyst is up to 93% (Fig. S3). After the durability test of the electrocatalyst for overall water splitting, the XRD, SEM, XPS, and EDS of MoSe$_2$-Ni$_3$Se$_2$/NF were tested. The results show that the structure and the surface morphology of the electrocatalyst roughly maintain the original characteristics (Figs. S4–S7).

4   Conclusions

The MoSe$_2$-Ni$_3$Se$_2$/NF heterogeneous composite was fabricated by utilizing a one-pot hydrothermal method. The MoSe$_2$-Ni$_3$Se$_2$/NF heterogeneous composite demonstrated an excellent electrocatalytic activity and a long-term stability for HER, OER, and total water splitting. When the sample was used as a bifunctional electrocatalyst to drive the electrocatalytic total water splitting, an overpotential of only 1.60 V is required at 10 mA/cm^2. Meanwhile, the catalyst demonstrated a satisfactory durability and an almost unchanged overpotential after a durability test of 80000 s. The increase in the catalytic activity of the electrocatalyst can be attributed to the fact that the introduction of the molybdenum source has caused the surface of the electrocatalyst to be reconstructed to form a heterogeneous structure, which increases the active sites on the electrocatalyst surface and accelerates the electron transport speed, thereby improving the electrocatalytic activity. In addition, with the introduction of the molybdenum source, a multi-component multi-interface electrocatalyst is formed, which may lead to an increase in the electrocatalytic activity. It is hoped that this work may provide a direction for the surface regulation of nanomaterials and the development of efficient dual-functional electrocatalysts.
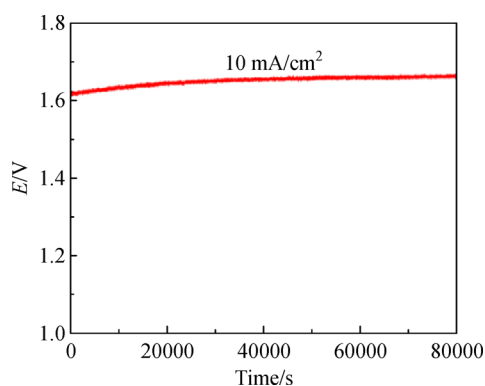
Fig. 9   Durability tests at 10 mA/cm^2 of MoSe$_2$-Ni$_3$Se$_2$/NF for total water splitting in lake water.

References

1. Bodhankar P M, Sarawade P B, Singh G, et al. Recent advances in highly active nanostructured NiFe LDH catalyst for electrochemical water splitting. Journal of Materials Chemistry A, 2021, 9(6): 3180–3208

2. Wang P, Jia T, Wang B. A critical review: 1D/2D nanostructured self-supported electrodes for electrochemical water splitting. Journal of Power Sources, 2020, 474: 228621

3. Zhao D, Zhuang Z, Cao X, et al. Atomic site electrocatalysts for water splitting, oxygen reduction and selective oxidation. Chemical Society Reviews, 2020, 49(7): 2215–2264

4. Han N, Liu P, Jiang J, et al. Recent advances in nanostructured metal nitrides for water splitting. Journal of Materials Chemistry A, 2018, 6(41): 19912–19933

5. Li S, Hao X, Abudula A, et al. Nanostructured Co-based bifunctional electrocatalysts for energy conversion and storage: current status and perspectives. Journal of Materials Chemistry A, 2019, 7(32): 18674–18707

6. Li Z, Ge R, Su J, et al. Recent progress in low Pt content electrocatalysts for hydrogen evolution reaction. Advanced Materials Interfaces, 2020, 7(14): 2000396

7. Weng C, Ren J, Yuan Z. Transition metal phosphide-based materials for efficient electrochemical hydrogen evolution: a critical review. ChemSusChem, 2020, 13(13): 3357–3375

8. Yang Z, Zhao C, Qu Y, et al. Trifunctional self-supporting cobalt-embedded carbon nanotube films for ORR, OER, and HER triggered by solid diffusion from bulk metal. Advanced Materials, 2019, 31(12): 1808043

9. Wang H, Fu W, Yang X, et al. Recent advancements in heterostructured interface engineering for hydrogen evolution reaction electrocatalysis. Journal of Materials Chemistry A, 2020, 8(15): 6926–6956

10. Ding W, Cao Y, Liu H, et al. *In situ* growth of NiSe@Co$_{0.85}$Se heterointerface structure with electronic modulation on nickel foam for overall water splitting. Rare Metals, 2021, 40(6): 1373–1382

11. Tang Y, Liu Q, Dong L, et al. Activating the hydrogen evolution and overall water splitting performance of NiFe LDH by cation doping and plasma reduction. Applied Catalysis B: Environmental, 2020, 266: 118627

12. Hua W, Sun H, Xu F, et al. A review and perspective on molybdenum-based electrocatalysts for hydrogen evolution reaction. Rare Metals, 2020, 39(4): 335–351

13. Yan P, Liu Q, Zhang H, et al. Deeply reconstructed hierarchical and defective NiOOH/FeOOH nanoboxes with accelerated kinetics for the oxygen evolution reaction. Journal of Materials Chemistry A, 2021, 9(28): 15586–15594

14. Sun H, Yan Z, Liu F, et al. Self-supported transition-metal-based electrocatalysts for hydrogen and oxygen evolution. Advanced Materials, 2020, 32(3): 1806326

15. Yao Q, Huang B, Zhang N, et al. Channel-rich RuCu nanosheets for pH-universal overall water splitting electrocatalysis. Angewandte Chemie International Edition, 2019, 58(39): 13983–13988

16. Tiwari A P, Kim D, Kim Y, et al. Highly active and stable layered ternary transition metal chalcogenide for hydrogen evolution reaction. Nano Energy, 2016, 28: 366–372

17. Du H, Kong R, Guo X, et al. Recent progress in transition metal phosphides with enhanced electrocatalysis for hydrogen evolution. Nanoscale, 2018, 10(46): 21617–21624

18. Ibraheem S, Li X, Shah S S A, et al. Tellurium triggered formation of Te/Fe-NiOOH nanocubes as an efficient bifunctional electrocatalyst for overall water splitting. ACS Applied Materials & Interfaces, 2021, 13(9): 10972–10978

19. Kim D, Qin X, Yan B, et al. Sprout-shaped Mo-doped CoP with maximized hydrophilicity and gas bubble release for high-performance water splitting catalyst. Chemical Engineering Journal, 2021, 408: 127331

20. Feng X, Shi Y, Shi J, et al. Superhydrophilic 3D peony flower-like Mo-doped Ni$_2$S$_3$@NiFe LDH heterostructure electrocatalyst for accelerating water splitting. International Journal of Hydrogen Energy, 2021, 46(7): 5169–5180

21. Tian Y, Xue X, Gu Y, et al. Electrodeposition of Ni$_3$Se$_2$/MoSe$_x$ as a bifunctional electrocatalyst towards highly-efficient overall water splitting. Nanoscale, 2020, 12(45): 23125–23133

22. Badrnezhad R, Nasri F, Pourfarzad H, et al. Effect of iron on Ni–Mo–Fe composite as a low-cost bifunctional electrocatalyst for overall water splitting. International Journal of Hydrogen Energy, 2021, 46(5): 3821–3832

23. Zhang R, Wang G, Wei Z, et al. A Fe–Ni$_5$P$_4$/Fe–Ni$_2$P heterojunction electrocatalyst for highly efficient solar-to-hydrogen generation. Journal of Materials Chemistry A, 2021, 9(2): 1221–1229

24. Barati Darband G, Aliofkhazraei M, Hyun S, et al. Pulse electrodeposition of a superhydrophilic and binder-free Ni–Fe–P nanostructure as highly active and durable electrocatalyst for both hydrogen and oxygen evolution reactions. ACS Applied Materials & Interfaces, 2020, 12(48): 53719–53730

25. Jeghan S M N, Kim J, Lee G. Hierarchically designed CoMo marigold flower-like 3D nano-heterostructure as an efficient electrocatalyst for oxygen and hydrogen evolution reactions. Applied Surface Science, 2021, 546: 149072

26. Zhao Y, Zhang J, Xie Y, et al. Constructing atomic heterometallic sites in ultrathin nickel-incorporated cobalt phosphide nanosheets via a boron-assisted strategy for highly efficient water splitting. Nano Letters, 2021, 21(1): 823–832

27. Lv X, Xiao Z, Wang H, et al. *In situ* construction of Co/N/C-based heterojunction on biomass-derived hierarchical porous carbon with stable active sites using a Co-N protective strategy for high-efficiency ORR, OER and HER trifunctional electrocatalysts. Journal of Energy Chemistry, 2021, 54: 626–638

28. Ma X, Li K, Zhang X, et al. The surface engineering of cobalt carbide spheres through N, B co-doping achieved by room-temperature *in situ* anchoring effects for active and durable multifunctional electrocatalysts. Journal of Materials Chemistry A, 2019, 7(24): 14904–14915

29. Geng B, Yan F, Liu L, et al. Ni/MoC heteronanoparticles encapsulated within nitrogen-doped carbon nanotube arrays as highly efficient self-supported electrodes for overall water splitting. Chemical Engineering Journal, 2021, 406: 126815

30. Hu E, Yao Y, Chen Y, et al. Boosting hydrogen generation by anodic oxidation of iodide over Ni–Co(OH)$_2$ nanosheet arrays. Nanoscale Advances, 2021, 3(2): 604–610

31. Rajesh J A, Jo I R, Kang S H, et al. Potentiostatically deposited bimetallic cobalt-nickel selenide nanostructures on nickel foam for highly efficient overall water splitting. International Journal of Hydrogen Energy, 2021, 46(10): 7297–7308

32. Yan H, Xie Y, Wu A, et al. Anion-modulated HER and OER activities of 3D Ni–V-based interstitial compound heterojunctions for high-efficiency and stable overall water splitting. Advanced Materials, 2019, 31(23): 1901174

33. Liu L, Yan F, Li K, et al. Ultrasmall FeNi$_3$N particles with an exposed active (110) surface anchored on nitrogen-doped graphene for multifunctional electrocatalysts. Journal of Materials Chemistry A, 2019, 7(3): 1083–1091

34. Zhu C, Yin Z, Lai W, et al. Fe-Ni-Mo nitride porous nanotubes for full water splitting and Zn-air batteries. Advanced Energy Materials, 2018, 8(36): 1802327

35. Wang Y, Liu J, Liao Y, et al. Hetero-structured V-Ni$_3$S$_2$@NiOOH core-shell nanorods from an electrochemical anodization for water splitting. Journal of Alloys and Compounds, 2021, 856: 158219

36. Li Z, Yang J, Chen Z, et al. V "bridged" Co–O to eliminate charge transfer barriers and drive lattice oxygen oxidation during water-splitting. Advanced Functional Materials, 2021, 31(9): 2008822

37. Jamesh M I. Recent progress on earth abundant hydrogen evolution reaction and oxygen evolution reaction bifunctional electrocatalyst for overall water splitting in alkaline media. Journal of Power Sources, 2016, 333: 213–236

38. D'Olimpio G, Nappini S, Vorokhta M, et al. Enhanced electro-catalytic activity in GaSe and InSe nanosheets: the role of surface oxides. Advanced Functional Materials, 2020, 30(43): 2005466

39. Yi X, He X, Yin F, et al. Amorphous Ni-Fe-Se hollow nanospheres electrodeposited on nickel foam as a highly active and bifunctional catalyst for alkaline water splitting. Dalton Transactions (Cambridge, England), 2020, 49(20): 6764–6775

40. He L, Cui B, Hu B, et al. Mesoporous nanostructured CoFe–Se–P composite derived from a Prussian blue analogue as a superior electrocatalyst for efficient overall water splitting. ACS Applied Energy Materials, 2018, 1(8): 3915–3928

41. Zhang Y, Qiu Y, Ji X, et al. Direct growth of CNTs@CoS$_x$Se$_{2(1-x)}$ on carbon cloth for overall water splitting. ChemSusChem, 2019, 12 (16): 3792–3800

42. Zhu J, Ni Y. Phase-controlled synthesis and the phase-dependent HER and OER performances of nickel selenide nanosheets prepared by an electrochemical deposition route. CrystEngComm, 2018, 20 (24): 3344–3352

43. Yang Y, Zhang K, Lin H, et al. MoS$_2$–Ni$_3$S$_2$ heteronanorods as efficient and stable bifunctional electrocatalysts for overall water splitting. ACS Catalysis, 2017, 7(4): 2357–2366

44. Yang Y, Zhao X, Mao H, et al. Nickel-doped MoSe$_2$ nanosheets with Ni–Se bond for alkaline electrocatalytic hydrogen evolution. International Journal of Hydrogen Energy, 2020, 45(18): 10724–10728

45. Zhong Y, Chang B, Shao Y, et al. Regulating phase conversion from Ni$_3$Se$_2$ into NiSe in a bifunctional electrocatalyst for overall water-splitting enhancement. ChemSusChem, 2019, 12(9): 2008–2014

46. Liu N, Yang L, Wang S, et al. Ultrathin MoS$_2$ nanosheets growing within an in-situ-formed template as efficient electrocatalysts for hydrogen evolution. Journal of Power Sources, 2015, 275: 588–594

47. Liu W, Yu L, Yin R, et al. Non-3d metal modulation of a 2D Ni–Co heterostructure array as multifunctional electrocatalyst for portable overall water splitting. Small, 2020, 16(10): 1906775

48. Zhang B, Xiao C, Xie S, et al. Iron–Nickel nitride nanostructures in-situ grown on surface-redox-etching nickel foam: efficient and ultrasustainable electrocatalysts for overall water splitting. Chemistry of Materials, 2016, 28(19): 6934–6941

49. Feng L L, Yu G, Wu Y, et al. High-index faceted Ni$_3$S$_2$ nanosheet arrays as highly active and ultrastable electrocatalysts for water splitting. Journal of the American Chemical Society, 2015, 137(44): 14023–14026

50. Shit S, Chhetri S, Jang W, et al. Cobalt sulfide/nickel sulfide heterostructure directly grown on nickel foam: an efficient and durable electrocatalyst for overall water splitting application. ACS Applied Materials & Interfaces, 2018, 10(33): 27712–27722

51. Liu J, Zhu D, Ling T, et al. S-NiFe$_2$O$_4$ ultra-small nanoparticle built nanosheets for efficient water splitting in alkaline and neutral pH. Nano Energy, 2017, 40: 264–273

52. Li J, Wei G, Zhu Y, et al. Hierarchical NiCoP nanocone arrays supported on Ni foam as an efficient and stable bifunctional electrocatalyst for overall water splitting. Journal of Materials Chemistry A, 2017, 5(28): 14828–14837

53. Chen T, Tan Y. Hierarchical CoNiSe$_2$ nano-architecture as a high-performance electrocatalyst for water splitting. Nano Research, 2018, 11(3): 1331–1344

54. Wang H, Sun Y, Ma F, et al. Se molarity tuned composition and configuration of Ni$_3$Se$_2$/NiSe core-shell nanowire heterostructures for hydrogen evolution reaction. Journal of Alloys and Compounds, 2020, 819: 153056